18
FERMILAB
MAR 15 2001
LIBRARY

GANIL

GANIL-P-01-03

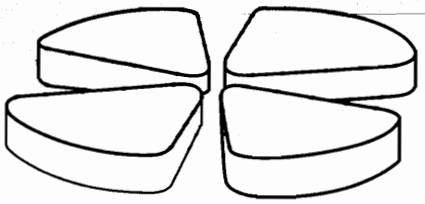

Shell structure of nuclei far from stability

H. Grawe[a] and M. Lewitowicz[b]

[a] Gesellschaft für Schwerionenforschung mbH, D-64291 Darmstadt, Germany
[b] Grand Accélérateur National d'Ions Lourds, BP 55027, F-14076 Caen, France

Fermilab Library
0 1160 0089627 8

Submitted to the Special Issue of Nuclear Physics A
"Research Opportunities with Accelerated Beams of Radioactive Ions"

GANIL P 01 03

Shell structure of nuclei far from stability

H. Grawe[a], M. Lewitowicz[b] *

[a]Gesellschaft für Schwerionenforschung mbH, D- 64291 Darmstadt, Germany

[b]Grand Accélérateur National d'Ions Lourds, BP 55027, F-14076 Caen, France

The experimental status of shell structure studies in medium-heavy nuclei far off the line of β-stability is reviewed. Experimental techniques, signatures for shell closure and expectations for future investigations are discussed for the key regions around ^{48,56}Ni, ^{100}Sn for proton rich nuclei and the neutron-rich N=20 isotones, Ca, Ni and Sn isotopes.

PACS: 21.10.Dr, 21.10.Pc, 21.60.Cs, 23.40.Hc, 29.30.-h.

Keywords: Shell model, shell closure, single particle energies, exotic nuclei.

1. Introduction

Doubly magic nuclei in exotic regions of the nuclidic chart are key points to determine shell structure as documented in single particle energies (SPE) and residual interaction between valence nucleons. The parameters of schematic interactions, entering e.g. the numerous versions of Skyrme-Hartree-Fock calculations, are not well determined by the spectroscopy of nuclei close to β-stability [1]. Relativistic mean field predictions are hampered by the delicate balance of single particle and spin-orbit potentials, which are determined by the small difference and the large sum, respectively, of the contributions from vector and scalar mesons [2]. Experimental SPE on the other hand, are often distorted by quadrupole and octupole correlations, which are not accounted for in mean field calculations. This prevents a direct comparison between experiment and theory. Modern realistic interactions as deduced from NN phase shifts by G-matrix many-body theory [3] account very well for the spectroscopy of nuclei [4–6] but need to be modified [7] to reproduce saturation. It has been pointed out recently that there is an intimate relation between correct reproduction of the spectroscopy of nuclei and the physics of neutron stars, mediated by the realistic interaction [8].

As a mandatory prerequisite to study the relation between nuclear spectroscopy and realistic interactions large scale shell model codes were developed, which enable a detailed comparison not only of level schemes but also of electromagnetic transition rates, Gamow-Teller strengths and even shape evolution up to ^{100}Sn [9,10]. Monte-Carlo shell model calculations have also become feasible for the region between ^{56}Ni, ^{78}Ni and ^{100}Sn [11–13].

Spectroscopic studies around the doubly magic nuclei ^{48,56}Ni and ^{100}Sn, at N=Z and the proton dripline, and ^{48}Ca, ^{78}Ni and ^{132}Sn at large N/Z ratios provide therefore an excel-

*E-mail: h.grawe@gsi.de, lewitowicz@ganil.fr

lent probe for shell structure, residual interaction, spin-isospin and shape correlations over the full range of nuclei accessible with state of the art experimental techniques. Recent progress in the development of efficient γ-arrays with highly selective ancillary detectors as operative in EUROBALL [14] and GAMMASPHERE [15] and the effective combination of highly efficient γ-detection with in-flight and on-line separators have enabled spectroscopy of these exotic regions of the Segré chart. These doubly magic nuclei, situated at key points of the rp– and r–paths, respectively, cover the full range in the ratio $0.7 \leq N/Z \leq 1.8$ that is available to probe the isovector part of the nuclear mean field, which is not determined by the large body of data available for less exotic nuclei.

This review will summarize the present knowledge of shell structure of medium heavy exotic nuclei between N=20 and 82 (fig. 1). The region below and beyond this range will be covered in other contributions to this volume.

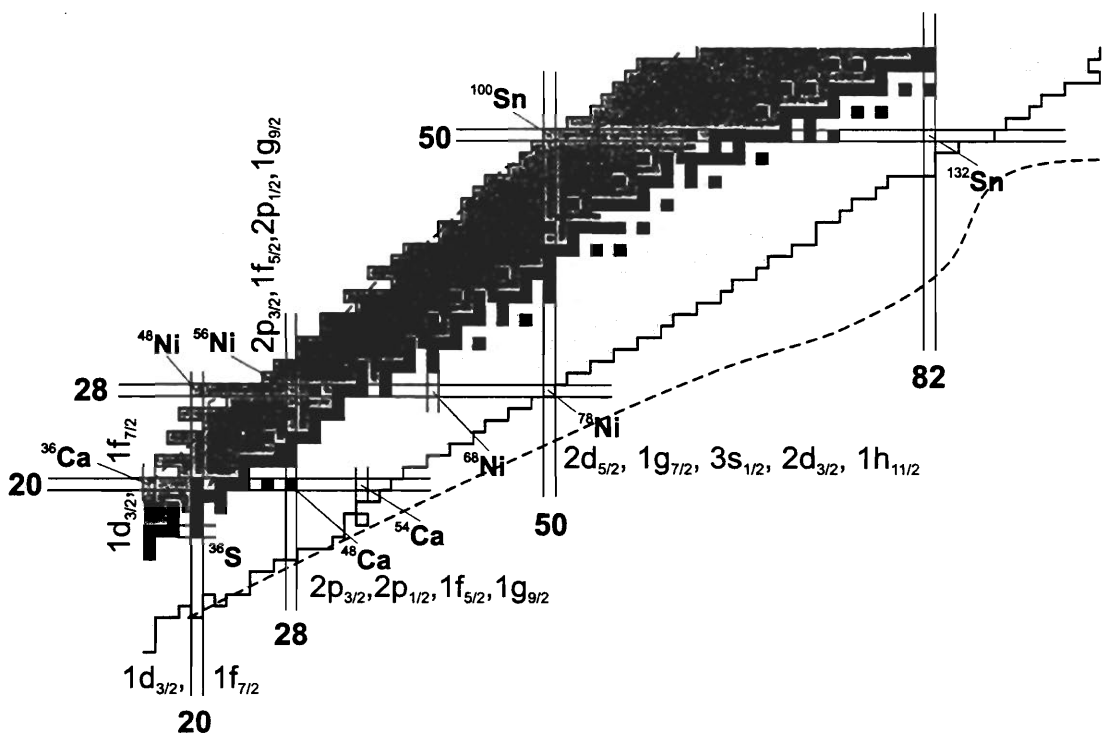

Figure 1. Section of the Segré chart covered in this article.

2. Experimental techniques

An already very broad spectrum of the experimental techniques used to explore the shell structure of nuclei far from stability was significantly enlarged in the recent years. The

extensive use of secondary beams issued from the projectile fragmentation reactions, a new generation of 4π γ, neutron and charged particle spectrometers as well as a significant improvement of highly selective ISOL and IGISOL methods serve as main tools of this rapid technical development. In the following section several examples illustrating the main tendencies in the recent experiments dedicated to the study of exotic nuclei between Ne and Sn are presented.

2.1. In-flight separation and identification of fast reaction products

In practically all recent applications using the projectile fragmentation to produce radioactive ions, magnetic spectrometers were used in combination with other solid state or gas detectors. These kind of experimental set-ups allows for an unambiguous, event-by-event identification of heavy ions up to about Z=50 and mass A=100 at intermediate energies and up to Uranium isotopes at several hundred MeV per nucleon. The radioactive beams formed in the fragment separators may serve for a time-of-flight based mass measurement [16], study of decay properties [17–19] or might induce secondary reactions. A detailed description of the most extensively used fragment separators and associated techniques may be found in ref. [20,21].

Magnetic spectrometers may be used very efficiently to select among all reaction products nuclei of interest produced with a counting rate as low as one event per day. The currently achieved lower limit of the measured production cross section is 0.05 pb [22]. In order to obtain this degree of selectivity the specific energy loss of heavy ions is used in the achromatic spectrometer. At intermediate energies, a further purification of secondary beams, specially on the proton-rich side, may be achieved by a velocity filter using crossed magnetic and electric fields. Three examples presented in the following illustrate main features of these techniques.

The doubly magic nucleus ^{100}Sn was produced in fragmentation of relativistic (^{124}Xe at 1095·A MeV) [23] and intermediate-energy (^{112}Sn at 63·A MeV) [24] heavy-ion beams and identified using fragment separator techniques.

In the experiment performed at GSI fragments produced in the interactions of a ^{124}Xe beam of 4x10^7 pps in a 6 g/cm^2 thick Be target were analysed by means of the fragment separator FRS. The ^{100}Sn nucleus was produced and clearly identified using ΔE, time-of-flight and Bρ measurements. Despite of a very low production rate for the most exotic nuclei, very selective implantation and a specially developed low background detection systems for β^+-decay enabled the first measurements of the half-lives of ^{100}Sn and other neighbouring nuclei. Recently a similar technique used in an experiment with a 1·A GeV ^{112}Sn beam allowed for a systematic measurement of half-lives for the N=Z nuclei between ^{77}Y and ^{98}In [25].

To produce and identify ^{100}Sn [24,26] and recently ^{48}Ni [22] at GANIL fragmentation-like reactions at several tens of MeV per nucleon were employed in conjunction with the SISSI superconducting solenoids and the magnetic spectrometers Alpha and LISE3 which provided the collection, separation and in-flight identification of the different reaction products. In order to enhance the production of neutron-deficient isotopes a beam of the lightest, stable tin or nickel isotopes (^{112}Sn and ^{58}Ni) with intensity of 2.4 pnA and 115 pnA respectively, on a natural Ni target (typically 0.2 g/cm^2 thick) were used. A schematic view of this complex but highly selective system is shown in figure 2.

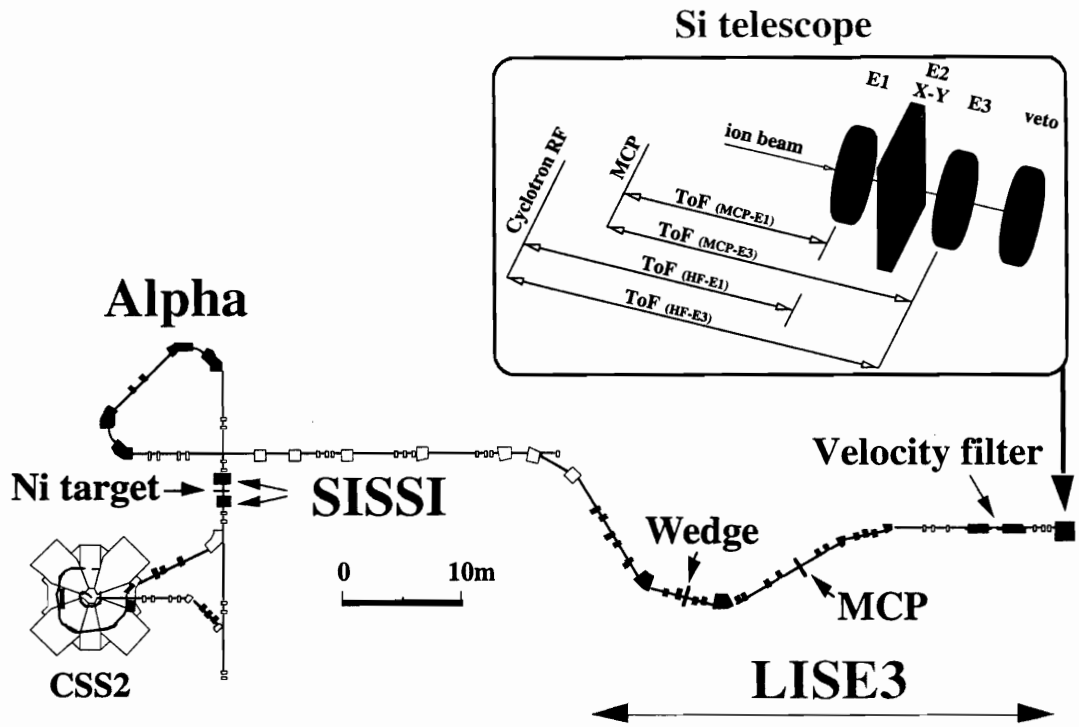

Figure 2. Experimental setup for in-flight identification and study of fragments used at GANIL. MCP stands for position sensitive micro-channel plate timing detector and CSS2 for the second sector separated cyclotron of the GANIL facility.

2.2. Decay study of short-lived isomers

Study of short-lived ($T_{1/2}$ about 0.1 to 100μs) isomeric states at intermediate and relativistic energies allows to combine an unambiguous and fast event-by-event identification of nuclei far from stability with a high-resolution γ-spectroscopy [27]. Since several years this experimental method is extensively used in order to map and study, so far inaccessible, regions of the chart of nuclei [28–32], on both, neutron and proton-rich sides.

Very recently, other experimental techniques namely Time Dependent Perturbed Angular Distribution (TDPAD) measurements with spin aligned nuclei, fast timing measurements as well as the conversion electron (CE) spectroscopy were successfully combined with the production of short-lived isomeric states at GANIL. In particular, the g-factor for the ^{67}Ni, $I^{\pi} = 9/2^{+}$ isomer produced in fragmentation of a ^{76}Ge, 61.4·A MeV beam on a ^{9}Be target was determined using the TDPAD method [33]. The measurement of conversion electrons allowed to confirm in a direct way, the existence of an isomeric 0^{+} state in ^{74}Kr. Moreover, a new 0^{+} isomer was identified as the first excited state of the N=Z nucleus ^{72}Kr [34]. Finally, the fast timing BaF_2-BaF_2 measurement in conjunction with the event-by-event identification of isomeric states produced at intermediate energies opened interesting possibilities to determine the lifetime of states populated in the decay of an isomer. In particular, in a recent experiment with the ^{76}Ge 60·A MeV beam several

sub-nanosecond lifetimes for levels in ^{70}Ni, ^{71}Cu, ^{69}Ni, and ^{67}Ni have been measured with high precision [35].

2.3. In-beam spectroscopy with primary and radioactive intermediate energy beams

The Coulomb excitation of fast fragments allowed during the last few years to measure in a systematic way excitation energies of the 2^+ states and the corresponding B(E2;$2^+ \rightarrow 0^+$) values for a large range of exotic even-even nuclei (see contribution of T. Glasmacher to this issue).

In order to observe the higher spin and higher excitation energy states in very exotic nuclei a new and original method was proposed recently at GANIL and RIKEN. Stable or radioactive neutron-rich beams at several tens of MeV per nucleon interact with a relatively thick Be or C target surrounded by high efficiency γ-ray detectors composed in an array of BaF_2, NaI or Ge clover detectors. The forward peaked reaction products are detected by means of a high acceptance magnetic spectrometer [36] or a silicon telescope [37] . The full and highly efficient identification of outgoing fragments allowed to observe clearly γ-transitions even for ions produced with a rate below 0.1 particle per second. A number of very neutron rich nuclei from oxygen to sulfur was explored in this way using ^{36}S and ^{48}Ca beams at GANIL.

Due to a high counting rate in the γ-ray detectors, in this kind of experiments the intensity of a stable beam is usually limited to about 1pnA. This problem might be solved if instead of the stable beam a radioactive one, issued from the fragmentation process, is used. The choice of the radioactive beam close in mass and charge to the nucleus of interest increases significantly the secondary reaction cross section. The first experiments using this approach were performed in order to study excited states in ^{34}Mg [37] and in nuclei in the vicinity of ^{24}O [38]. A very similar technique is applied to study nuclear structure via knock-out reactions (see contribution of B. Sherrill and P. G. Hansen to this issue).

2.4. In-beam and decay spectroscopy at Coulomb barrier energies

For in-beam spectroscopy of exotic nuclei, produced below the mb level of cross sections in fusion-evaporation, besides efficient γ- detection in arrays like GAMMASPHERE [15] and EUROBALL [14] highly efficient, selective and versatile ancillary detectors are required. They serve both, as filter to discriminate against abundantly produced less exotic species and for exit channel identification of unknown nuclides. In fig. 3 a typical setup used at EUROBALL is shown schematically. With setups of similar performance in-beam γ-ray spectroscopy is possible down to the μb level, which corresponds to $<10^{-5}$ of the total residue production or a production rate of $\sim$ 1 atom/s. Neutron-rich nuclei are produced in spontaneous and heavy- ion induced fission and by inelastic collisions. Selection and identification of the binary reaction products rely entirely on efficient detection of high-fold γ-coincidences, advanced ancillary devices were used to date only in few cases (see for example [39]).

In β-decay studies only recently the power of large high-resolution γ-arrays as a Ge-cluster cube [41] in combination with a high-efficiency total absorption spectrometer (TAS) [41,42] was demonstrated, setting a new landmark for modern detection devices.

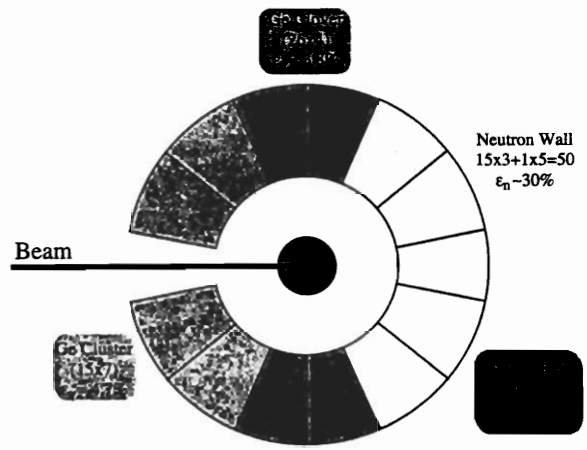

Figure 3. Schematic experimental setup for in-beam spectroscopy of neutron- deficient nuclei at EUROBALL [14], comprising 3π of Compton suppressed Ge-detectors, the Si-telescope ball ISIS [40] for charged particle and the neutron wall [43] for neutron detection.

3. Experimental signatures for (sub)shell closure

The most sensitive and direct signature for (sub)shell closures can be derived from binding energies. The second difference

$$\delta_{2n} = S_{2n}(Z,N+2) - S_{2n}(Z,N) \tag{1}$$

as calculated from the binding energy BE

$$S_{2n}(N) = BE(Z,N+2) - BE(Z,N) \tag{2}$$

and correspondingly for δ_{2p} and S_{2p} shows a distinct peak for closed shell nuclei and its height represents the shell gap. It should be noted, however, that a basic change of the underlying nuclear structure, as e.g. quadrupole or octupole correlations, can severely distort δ, as the binding energies of three nuclei are involved in eq. (1) (see also subsect. 5.3). More indirect measures for shell closures, though even more affected by structure effects, are the excitation energies of $I^\pi=2^+$ states $E(2^+)$ and the γ-transition strength $B(E2;2^+ \rightarrow 0^+)$. In figs. 4-6 δ_{2n}, $E(2^+)$ and B(E2) values are shown for the series of semi-magic Ca, Ni and Sn isotopes (full circles and lines). The data are taken from the Nuclear Data Sheets (NDS), the compilations as cited in ref. [44] and recent data referred to elsewhere in this review. For $N \leq Z$, because of scarce data and to demonstrate isospin symmetry, the corresponding δ_{2p}, $E(2^+)$ and B(E2) values for the mirror nuclei, the N=20,28 and 50 isotones, are shown (open circles, dashed lines). In the overlapping regions mirror symmetry is clearly exhibited, the difference in the B(E2) values being due to the isovector part of the E2 operator.

In the following sections we will discuss the shell structure in specific regions of medium

heavy exotic nuclei.

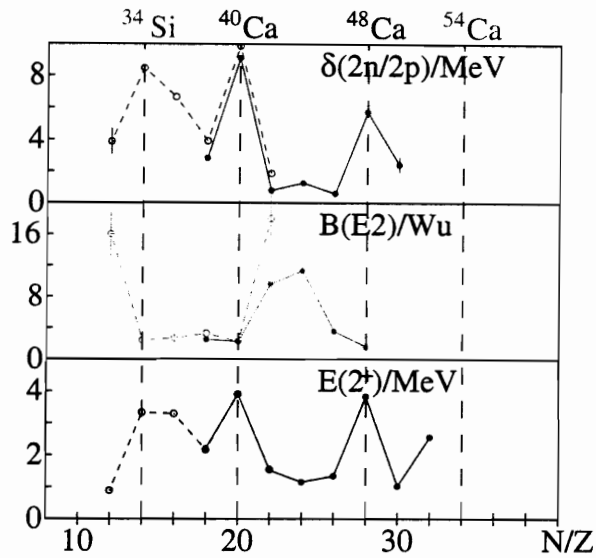

Figure 4. Excitation energies of the 2^+ states, the E2 strengths $B(E2;2^+ \rightarrow 0^+)$ and the second difference of the g.s. binding energies δ_{2n} resp. δ_{2p} for the Ca isotopes and the N=20 isotones, which are the isospin mirrors to the N≤Z Ca isotopes. Note the evidence for (sub)shell closures at N,Z = 14,16 (^{34}Si, ^{36}S) and N=34,(36) ($^{52,(54)}$Ca).

4. Proton-rich doubly magic nuclei from ^{48}Ni to ^{100}Sn

On the proton-rich side of the Segré chart shell structure is landmarked by the double shell closures at $^{48}_{28}Ni_{20}$, and the N=Z nuclei $^{56}_{28}Ni_{28}$ and $^{100}_{50}Sn_{50}$. They are situated at or close to the nucleosynthesis rp-path and the proton dripline which crosses the N=Z line at ^{100}Sn. Experimentally, only the ^{56}Ni region is studied well, whereas ^{48}Ni [22] and ^{100}Sn [23,24] nuclei were observed in a few events only. The stabilisation by the Coulomb barrier, however, may enable in the future detailed spectroscopy studies of ^{48}Ni and ^{100}Sn, too.

4.1. ^{48}Ni

The doubly magic nucleus was identified recently in few events following fragmentation of ^{58}Ni at the LISE spectrometer at GANIL [22]. With this discovery the Ni isotopic chain is the only one to host three doubly magic nuclei ^{48,56}Ni and ^{78}Ni (sect. 5.3). With T_z=-4 ^{48}Ni is the most neutron-deficient nucleus known to date, and the only doubly-magic nucleus with a known mirror partner $^{48}_{20}Ca_{28}$. It is predicted particle unstable, and as an even-Z nucleus it should decay by two-proton emission. The experimental half-life limit $t_{1/2} > 0.5\mu s$ and a decay energy of $Q_{2p} = 1.3$ MeV, as predicted by a number of mass

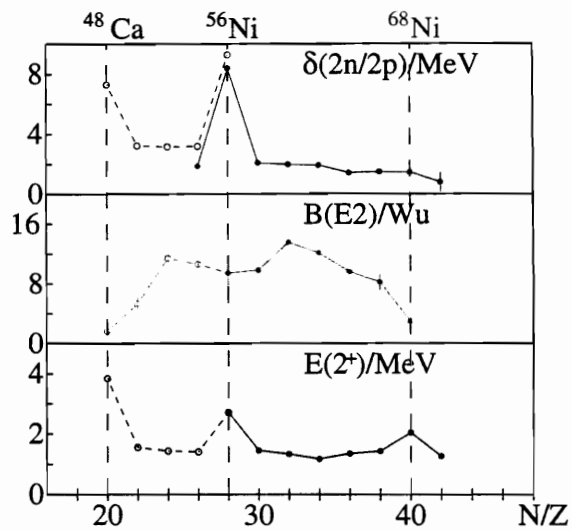

Figure 5. Excitation energies of the 2^+ states, the E2 strengths B(E2;$2^+ \rightarrow 0^+$) and the second difference of the g.s. binding energies δ_{2n} resp. δ_{2p} for the Ni isotopes and the N=28 isotones, the isospin mirrors to the N$\leq$Z Ni isotopes. Note the contradictory evidence for a N=40 shell from E(2^+), B(E2) and δ_{2n} in ^{68}Ni.

models, would allow for observation of this decay mode, as the partial β-decay half-life is expected to be greater than 6 ms [22].

The mirror pair ^{48}Ni - ^{48}Ca offers the unique chance to study isovector effects in the full $1f_{7/2}$ shell. As can be seen from fig. 4 isospin symmetry is nicely exhibited in the overlapping region around the self-conjugate nucleus $^{40}_{20}Ca_{20}$. Experimentally little structure information is known beyond the N=Z line from ^{40}Ca to ^{56}Ni. Recently the first detailed in-beam data on the T_z=-1 nucleus ^{50}Fe were obtained at EUROBALL [45], which will allow further detailed analysis of Coulomb shifts as a signature for changing intrinsic structure [46], and provide another benchmark for the power of the (f,p) shell model accounting for deformation and alignment [47]. It is a challenge for future experiments to study the N=14,16 subshell closure in the ^{34}Si, ^{36}S mirrors ^{34,36}Ca (see fig. 4). The lightest Ca isotope with detailed spectroscopy is ^{38}Ca [48]. A measured value for the E(2^+) in the proton unbound ^{32}Ca, would be the ultimate test whether the collectivity of ^{32}Mg is caused primarily by a N=20 shell quenching due to a diffuse neutron potential, or whether it is mainly due to *2p2h* excitation across the neutron shell, as observed in other midshell semimagic nuclei as e.g. ^{188}Pb [49].

4.2. ^{56}Ni

The shell closure at Z=N=28 is characterized by a large shell gap and E(2^+), but also a large B(E2; $2^+ \rightarrow 0^+$) [50], as shown in fig. 5. This is due to the *ls*-open core, which allows stretched $1f^{-1}_{7/2}\ 2p_{3/2}$ E2 excitations across the shell. It was shown in large scale shell model calculations [51] and in the Monte-Carlo shell model approach [13] in the full (f,p) shell,

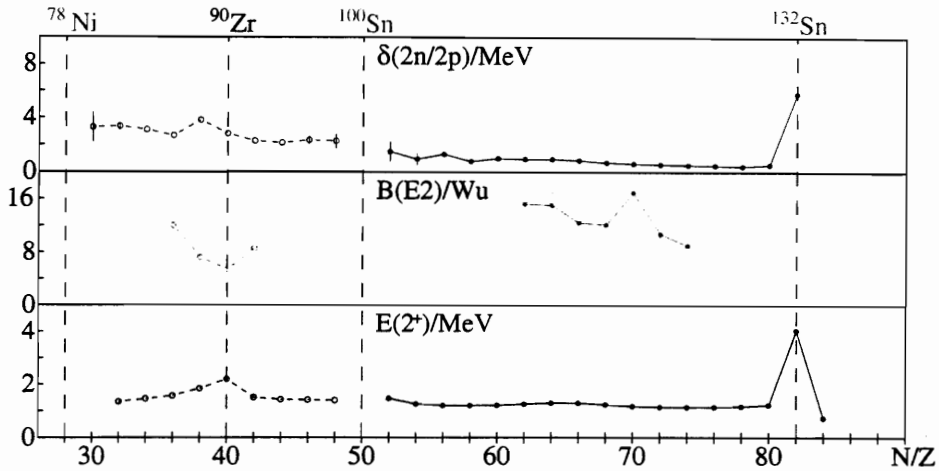

Figure 6. Excitation energies of the 2^+ states, the E2 strengths B(E2;$2^+ \rightarrow 0^+$) and the second difference of the g.s. binding energies δ_{2n} resp. δ_{2p} for the Sn isotopes and the N=50 isotones, the isospin mirrors to the N$\leq$Z Sn isotopes. Note the known (sub)shell closures at Z = 38,40 (^{88}Sr, ^{90}Zr).

that the closed shell configuration $1f^{16}$ covers only 50-60% of the ^{56}Ni ground state, the rest being up to *8p8h* excitations. The (f,p) shell model accounts well for spectroscopic data, deformation and B(E2) values with common polarisation charges of $\delta e_\pi = \delta e_\nu = 0.5\ e$ [51], and Gamow-Teller (GT) strengths and distribution with a general quenching factor (g_A/g_V)=0.74 $(g_A/g_V)_{free}$ [52].

The single particle (hole) energies in ^{56}Ni are well known as shown in fig. 7, with the $\nu g_{9/2}$ assigned recently [53]. The single particle spectrum of ^{56}Ni besides the afore mentioned susceptibility to E2 excitations, giving rise to deformed band structures on excited states [55], favors also $1f_{7/2}^{-1}\ 1f_{5/2}$ spin-flip excitations, which should strongly influence GT transitions, M1 transitions and g-factor core polarisation. The GT decay of ^{56}Cu was studied in a high resolution experiment [56], yielding good agreement with shell model predictions. The β^+/EC-decay from ^{57}Zn populates preferably single particle and simple core-excited states in ^{57}Cu, which were studied recently in β-delayed proton emission, which provides an alternative access to the ^{56}Ni shell structure [57]. The close lying proton dripline documents itself also in the observation of γ-delayed particle emission from excited states in ^{58}Cu [58] and ^{56}Ni [59], which is discussed in more detail in a different contribution to this volume [55].

4.3. ^{100}Sn

The experimental spectroscopic approach to ^{100}Sn is landmarked by the observation of excited states in its T_z=1 and 3/2 neighbours ^{98}Cd [60], ^{102}Sn [61] and ^{103}Sn [62,63]. Fig. 6 clearly demonstrates the need for spectroscopy and precise mass data for ^{100}Sn and its neighbours. While the mass of ^{100}Sn was measured with large statistical systematic uncertainty [64], nothing is known for its one- and two-particle (hole) neighbours. There-

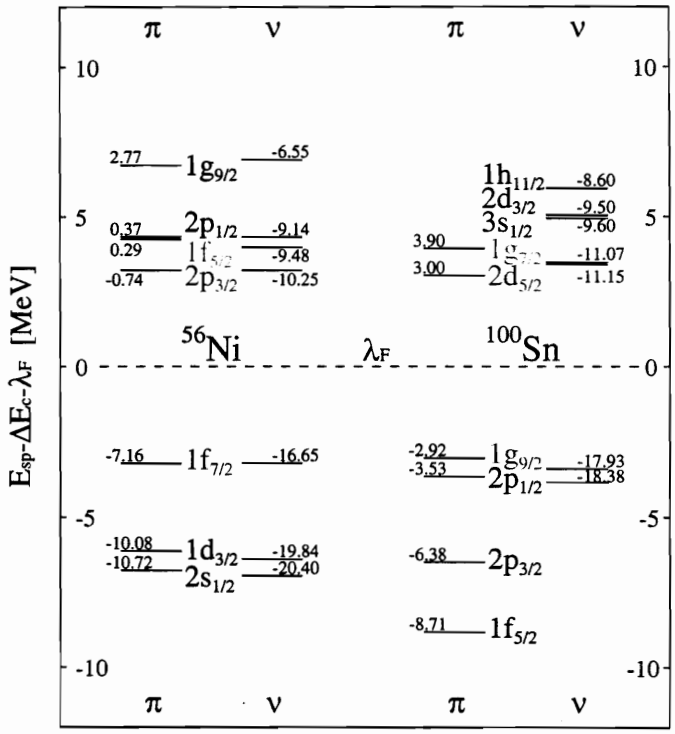

Figure 7. Single particle (hole) energies in ^{56}Ni and ^{100}Sn. The data are from NDS and ref [54].

fore the single particle (hole) energies for ^{100}Sn have to be inferred from more remote neighbours by a shell model analysis in an appropriately large model space, using realistic interactions. The method of extrapolation has been described in various publications [65–67] and the results are shown in fig. 7 in comparison to ^{56}Ni. While the hole $p_{1/2}$, $g_{9/2}$ and neutron particle $d_{5/2}$, $g_{7/2}$ energies close to the Fermi surface are accurate to about 100 keV, the shell gaps, the low spin neutron $s_{1/2}$, $d_{3/2}$, the $h_{11/2}$ and the proton particle energies have uncertainties of 300-500 keV. The recent data on quasiparticle states in ^{97}Pd [41], ^{99}Cd [69] and ^{103}Sn [62,63] are well accounted for by the choice of SPE shown in fig. 7 [65,67]. The close resemblance of shell structure between ^{56}Ni and ^{100}Sn, differing by one major shell, is nicely exhibited in fig. 7. Therefore similar structure effects as established for ^{56}Ni, such as E2 and spin-flip polarisability, are expected for ^{100}Sn, too. It was shown, that the extreme polarisation charges found for ^{98}Cd [60,68] and ^{102}Sn [61] can be reproduced in large scale shell model calculations allowing for up to *4p4h* excitations in a (g,d,s) model space, which is the limit of present state shell model calculations [9,65,67]. Consequently, a low-lying $I^{\pi}=2^{+}$ state with large B(E2) to the g.s. is expected for ^{100}Sn. Moreover, the shell structure of ^{100}Sn allows for enhanced stretched E3 transitions $p^{-1}_{1/2}$ $g_{7/2}$ ($l_2 - l_1$=3) and $p^{-1}_{1/2}$ $d_{5/2}$ ($l_2 + l_1$=3), as found in ^{104}Sn [70].

The β^{+}/EC-decay at ^{100}Sn is governed by the $\pi g_{9/2} \rightarrow \pi g_{7/2}$ GT transition. In modern experiments using high-efficiency γ-arrays or total absorption spectrometers (TAS) the

full GT strength of the GT resonance in the Q_{EC} window can be observed as shown in a pioneering experiment on the ^{97}Ag decay [41]. The observed quenching factor h=B(GT)$_{SM}$/B(GT)$_{EX}$ $\sim$ 3 - 4 can be factorised into a higher order correction $h_{high} \simeq$ 1.75 and a model space dependent part $h_{low} \sim$ 1.5 - 2.5, which contains core polarisation and can in principal be calculated in a *npnh* shell model calculation or a Monte-Carlo shell model approach [41,11,12].

Shell model calculations from the early days of empirical interactions in small model spaces [71–74] via inclusion of realistic interactions based on G-matrix many-body theory [75,3,76] in intermediate model spaces [77,65,78] to finally inclusion of up to $4p4h$ excitations [9,10] have been able to account for the experimental data around ^{100}Sn, such as excitation energies, GT-distributions, B(E2) and B(M1) values, with ever increasing accuracy.

5. Neutron-rich shell closures from ^{34}Si to ^{132}Sn

At N $\gg$ Z the disappearance of the familiar Woods-Saxon shell closures and their reappearance as harmonic oscillator magic numbers is a burning question, which is strongly related to the dilute neutron density and the decoupling of proton and neutron motion in weakly bound systems [79]. In this region of neutron-rich nuclei beyond the "halo" region, where the dripline is reached, double shell closures are unambiguously identified in figs. 4 - 6 for ^{34}Si/^{36}S at N=20, Z=14/16, $^{48}_{20}$Ca$_{28}$ and $^{132}_{50}$Sn$_{82}$. There is incomplete or controversial evidence for ^{52,54}Ca, ^{68}Ni and ^{78}Ni, which will be discussed below. The former group of nuclei is well studied in recent years, while little is known about the candidates of the latter group, of which ^{78}Ni was identified at GSI in 3 events following fission of relativistic ^{238}U [80]. ^{78}Ni and ^{132}Sn lie at keypoints of the nucleosynthesis r-path, which adds to their importance as benchmarks for nuclear structure at extreme neutron excess.

5.1. ^{34}Si, ^{36}S and the deformed ^{32}Mg

The N=20 isotones ^{34}Si and ^{36}S are known to exhibit features of a double shell closure with a δ_{2p} even larger than δ_{2n} for ^{48}Ca (fig. 4). They are separated by the $\pi s_{1/2}$ shell, which creates a situation similar to the pair of nuclei ^{88}Sr/^{90}Zr and ^{52,54}Ca (see next section). The structure of ^{34}Si, ^{36}S and the deformed ^{32}Mg [81] is well understood in large scale shell model [82] and Monto-Carlo shell model [83] calculations in a (s,d)+ν(p,f) model space. The reduced neutron shell gap is aiding the development of the "island of inversion" at ^{32}Mg as can be inferred from the δ_{2n} values across the N=20 shell. They drop from 9.1 MeV at the doubly magic ^{40}Ca to 1.2 MeV for ^{32}Mg. A detailed spectroscopy of the mirror Ca isotopes (sect. 4.1) would give deep insight into the isovector part of the nuclear mean field.

5.2. ^{48}Ca and ^{52,54}Ca

The shell closure at ^{48}Ca has been extensively studied in transfer reactions resulting in the single particle (hole) energies shown in fig. 8. It is worth to notice the difference in the neutron SPE for ^{56}Ni (fig. 7) at N=Z and ^{48}Ca at N/Z=1.4 . The neutron shell gap seems to be reduced in ^{48}Ca, but there is, however, the reversed effect on the spin-orbit splitting. The neutron SPE are mainly affected by the filling resp. emptying of the proton $1f_{7/2}$ shell going from ^{48}Ca to ^{56}Ni or vice versa, which causes a large monopole shift of

the $1f_{5/2}$ orbital. This shift would counteract an opening of a N=40 subshell between $1f_{5/2}$ and $1g_{9/2}$ going from ^{68}Ni to ^{60}Ca (see next section for a discussion of a N=40 shell gap). On the other hand, a reduction of the 2p spin-orbit splitting for the heavier neutron-rich Ca isotopes could open a gap between $2p_{1/2}$ and $1f_{5/2}$ at N=34. Indeed the steep rise of E(2^+) seems to support the appearance of a (sub)shell closure, which as in ^{34}Si/^{36}S at N=14/16 or ^{88}Sr/^{90}Zr at Z=38/40 is distributed over two nuclei. This is due to the presence of a $p_{1/2}$ resp. $s_{1/2}$ subshell, which is not coupled to the quadrupole properties shown in the lower panels of figs. 4-6 . Shell model calculations seem, at least partly, to account for this rise in ^{52}Ca [10,85], which should increase towards ^{54}Ca. This is again clearly a region where more experimental data are needed.

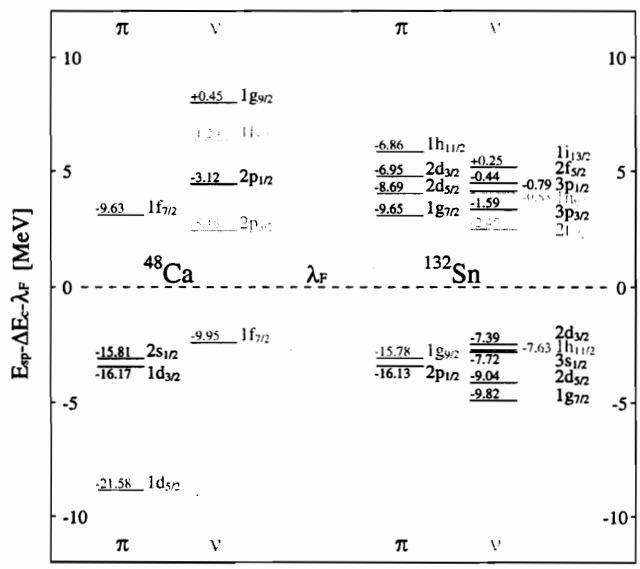

Figure 8. Single particle (hole) energies in ^{48}Ca and ^{132}Sn. The data are from NDS and refs. [54,84]. Note the correspondence of orbitals separated by two major shells, proton $1d_{5/2}$ - $1g_{9/2}$ and $1f_{7/2}$ - $1h_{11/2}$, and neutron $1f_{7/2}$ - $1h_{11/2}$, $2p_{3/2}$ - $2_{f7/2}$, $1f_{5/2}$ - $1h_{9/2}$, which allow an interpolation to the hitherto unknown ^{78}Ni shell structure.

5.3. ^{68}Ni and ^{78}Ni

Recent experimental data provide evidence on the N=40 and N=50 shell gaps at ^{68}Ni and ^{78}Ni, respectively. The experimental approach to ^{78}Ni is landmarked by the in-flight identification in a few events in relativistic fission [80] and by isomer and β-decay spectroscopy of ^{70}Ni [28], ^{73}Cu [86] and ^{78}Zn [87]. Beyond $^{68}_{28}$Ni$_{40}$ the filling of the $\nu g_{9/2}$ shell from ^{70}Ni to ^{76}Ni should give rise to a series of $I^{\pi}=8^+$ isomers, which sofar was identified in ^{70}Ni in fragmentation of ^{86}Kr [28] and ^{76}Ge [32] beams. ^{76}Ni is not accessible yet for spectroscopy studies but an identical isomer was discovered in its isotone ^{78}Zn [87]. This is firm evidence that the N=50 shell gap persists at ^{78}Ni as the cross shell excitation

would destroy the isomerism. Shell model calculations with the full $\pi\nu(p_{3/2}, f_{5/2}, p_{1/2}, g_{9/2})$ model space beyond ^{56}Ni account well for the spectroscopy and B(E2) values for Ni, Cu and Zn nuclei beyond N=40 [67,88]. Surprisingly the existence of an isomer in ^{72}Ni, analogue to ^{70}Ni, in a recent experiment could be excluded in the range 20 ns $\leq t_{1/2} \leq$ 2.5 ms [67]. This could be due to a distortion of the seniority scheme in mid-shell Ni isotopes, which has not been observed sofar for high-spin orbitals in the Segré chart [67].

It has been frequently invoked that the N=40 shell closure is well developed in ^{68}Ni [39,89,90]. More recently experimental evidence from β-decay was discussed [91,92] and a subtle balance of a possible shell gap and the pairing gap was made responsible for the controversial experimental evidence. The experimental facts are summarized in fig.5. ^{68}Ni has a large E(2^+) and a small B(E2;$2^+ \rightarrow 0^+$) [93], but no peak in δ_{2n}. Alternative explanations were given recently [65,94]. First, when the filling of the odd-parity (f,p) orbitals reaches the intruder $g_{9/2}$, in order to maintain parity at least two neutrons have to be excited to create a 2^+ state, while the E2 back-decay is particle forbidden. This was shown in a schematic way, assuming degenerate (f,p) orbitals and varying the $g_{9/2}$ by small amounts [67]. Most mean field calculations, on the other hand, produce distinct δ_{2n} peaks at N=40 (fig. 9, upper panel). Inclusion of quadrupole correlations make the peak disappear (fig. 9, lower panel) [94], which is due to the additional contribution to the g.s. energy of the ^{68}Ni neighbours by deformation. Note, that three g.s. masses are involved in calculating δ_{2n}. This raises the basic question to what extent experimental SPE and shell gaps can be compared to mean field predictions, which neglect correlations.

As masses and excited levels in the particle (hole) neighbours of ^{78}Ni are not known experimentally, single particle (hole) energies have to be inferred from extrapolations. For neutron holes along Z=28 isotopes the shell model extrapolation as described for ^{100}Sn is unreliable due to the distortion of the seniority scheme in midshell $\nu g_{9/2}$ [67]. For proton particles extrapolations along the N=50 isotones [74,75] and the Cu isotopes [88,86] yield the level sequence $f_{5/2}$, $p_{3/2}$, $p_{1/2}$, $g_{9/2}$, but the values are largely deviating. The most reliable estimate can be obtained from an interpolation of the corresponding ^{48}Ca and ^{132}Sn SPE shown in fig. 8, as e.g. $1f_{7/2} - 1g_{9/2} - 1h_{11/2}$ for neutron holes and proton particles, $1f_{5/2} - 1g_{7/2} - 1h_{9/2}$ for spin-orbit splitting and 2p – 2d – 2f for proton particles for ^{48}Ca – ^{78}Ni – ^{132}Sn, respectively [95].

5.4. ^{132}Sn

The two doubly magic Sn nuclei ^{100,132}Sn cover the whole range from exotic proton-rich N=Z nuclei across the valley of stability to exotic neutron-rich nuclei with N/Z>1.6 . Exploiting the fission process from the pioneering β-decay studies of high-spin parents [96,97] via prompt γ-decay studies of fission fragments [98,99] to isomer studies of fission fragments [100,101] a wealth of spectroscopy data were obtained. Almost all single particle (hole) energies are measured as shown in fig. 8 and a number of empirical two-particle (hole) and particle-hole multiplets were identified [98]. It should be noted though, that no spectroscopic factors are measured, which adds some uncertainty to the centroid position of the spectroscopic strength. The structure of ^{132}Sn in SPE, two-body matrix-elements (TBME) and core excitations shows almost a one-to-one correspondence to ^{208}Pb, when appropriately scaled [102,103]. The challenge for future experiments lies in the scanning of the N=82 isotones below Z=50 towards the r-path nuclei, where indirect evidence for

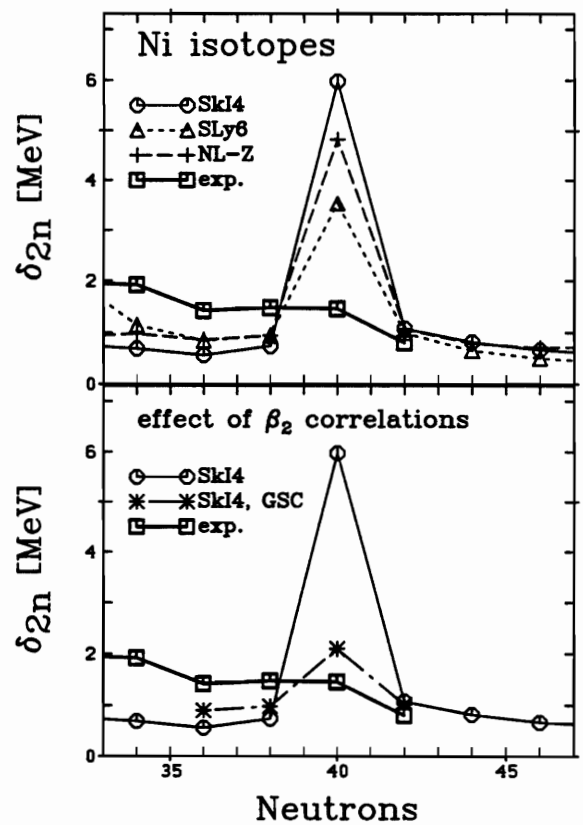

Figure 9. Second difference of the g.s. binding energies $\delta_{2n)}$ for Ni isotopes in various mean field approaches without (upper panel) and with quadrupole correlations (lower panel).

shell quenching was inferred [50], and in the investigation of the heavy Sn isotopes for the onset of deformation. Note, that ^{134}Sn has the lowest E(2^+) measured for a semi-magic nucleus in the chart of nuclides.

6. Conclusion and future perspectives

Great progress was made in the recent years in the study of nuclear shell structure by the development of ingenious detection techniques. Nevertheless, with respect to new shell structure this is just the first glimpse of what may happen far off the line of β-stability. Present experimental techniques are often at their limit, so only indirect experimental signatures for new shell structure are available for the most exotic regions. Even for the easily accessible doubly magic regions at ^{56}Ni and ^{132}Sn, spectroscopic factors are hardly known. The next step forward will be provided by radioactive beam facilities, those ready to operate as SPIRAL and REX-ISOLDE and those in the design or construction phase at RIKEN, GSI and in the US. The beam intensities foreseen for these facilities will allow to map the proton dripline up to lead (Z=82) and to study neutron-rich nuclei up to A/Z$\simeq$3,

which covers the full rp-path of nucleosynthesis and approaches the r-path between N=82 and 126.

Acknowledgment The authors enjoyed numerous and fruitful discussions with their colleagues from experiment and theory, and gratefully acknowledge the contribution of numerous postdocs and graduate students to the wealth of existing data on shell structure far from stability. Major contributions to the data presented in this review are from collaborations at EUROBALL, GAMMASPHERE, GANIL, GSI, ISOLDE, MSU and RIKEN.

REFERENCES

1. B.A. Brown, Phys. Rev. C58 (1998) 220
2. P. Ring, Progr. Part. Nucl. Phys. 37 (1996) 193
3. M. Hjorth-Jensen et al., Phys. Rep. 261 (1995) 125
4. T. Engeland et al., Phys. Rev. C61 (2000) 021302(R)
5. A. Covello et al., Proc. 6th Int. Spring Seminar on Nuclear Physics - " Highlights of modern nuclear structure", ed. A. Covello, World Scientific, Singapore, 1999, p.129
6. E. Caurier et al., Phys. Rev. Lett. 75 (1995) 2466
7. A. Poves and A.P. Zuker, Phys. Rep. 70 (1981) 235
8. H. Heiselberg, M. Hjorth-Jensen, Phys. Rep. 328 (2000) 237
9. F. Nowacki, Proc. SM2K, Nucl. Phys. A, in print
10. E. Caurier and G. Martínez-Pinedo, Proc. SM2K, Nucl. Phys. A, in print
11. D. Dean et al., Phys. Lett. B367 (1996) 17
12. S.E. Koonin et al., Phys. Rep. 278 (1997) 1
13. T. Otsuka et al., Phys. Rev. Lett. 81 (1998) 1588
14. C. Rossi-Alvarez, Proc. 6th Int. Spring Seminar on Nuclear Physics - " Highlights of modern nuclear structure", ed. A. Covello, World Scientific, Singapore, 1999, p.477
15. I.Y. Lee, Progr. Part. Nucl. Phys. 38 (1997) 65
16. W. Mittig, A.Lepine-Szily, N.A.Orr , Ann.Rev.Nucl.Part.Sci. 47 (1997) 27
17. Proc. Experimental Nucl. Physics in Europe, Sevilla, Spain, June 1999, eds B. Rubio, M. Lozano and W. Gelletly, AIP Conf. Proc. 495 (1999)
18. Proc. Workshop on beta decay, Strasbourg, France, March 1999, eds. P. Dessagne, A. Michalon, C. Miehe, IReS, Strasbourg, 1999
19. O. Sorlin et al., Proceedings of the Nuclear Structure 2000 conference, 15-19 August 2000, East Lansing, USA
20. A.M. Mueller and B.M. Sherrill, Ann.Rev.Nucl.and Part.Science 46 (1988)71
21. B.M. Sherill, Proc. of the Second Intern. Conf. on Radioactive Nuclear Beams, Louvain-la-Neuve, Belgium, 19-21 August 1991, Ed. Th. Delbar, IOP Publishing, p. 3
22. B. Blank et al., Phys. Rev. Lett. 84 (2000) 1116
23. R. Schneider et al., Z. Phys. A348 (1994) 241
24. M. Lewitowicz et al., Phys. Lett. B332 (1994) 20
25. E. Wefers et al., GSI Scientific Report 1999, GSI Report 2000-1 (2000) 23
26. K. Rykaczewski et al., Phys. Rev. C 52 (1995) R2310
27. R. Grzywacz et al., Phys. Lett. B 355 (1995) 439

28. R. Grzywacz et al., Phys. Rev. Lett. 81 (1998) 766
29. M. Pfützner et al., Phys. Lett. B 444 (1998) 32
30. J.-M. Daugas et al., Phys. Lett. B 476 (2000) 213 and references there in
31. C. Chandler et al., Phys. Rev. C 61(2000) 044309 and references there in
32. M. Lewitowicz et al., Proc. of the Nuclear Structure 2000 conference ,15-19 August 2000, East Lansing, USA, to be published in Nucl. Phys. A, see also http:// www.nscl.msu.edu/ conferences/ NS2000/ npa/ lewitowicz.pdf
33. G. Neyens et al., Proc. of the Nuclear Structure 2000 conference ,15-19 August 2000, East Lansing, USA
34. F. Becker et al., Abstract submitted to the Nuclear Structure at the Borderlines Conference Lipari, Italy May 2001
35. H. Mach et al., Abstract at the EPS 17th Int. Nucl. Phys. Conf., Eilat, Israel, January 17-19, 2001
36. M. Belleguic et al., Proc. of the Nuclear Structure 2000 conference ,15-19 August 2000, East Lansing, USA
37. K. Yoneda et al., Phys. Lett. B499 (2001) 233 and M. Ishihara, Proceedings of the Nuclear Structure 2000 conference ,15-19 August 2000, East Lansing, USA
38. M. Stanoiu et al. to be published in the Proc. of the XXXIX Intern. Winter Meeting on Nucl. Phys. Bormio, Italy, January 2001
39. T. Ishii et al., Phys. Rev. Lett. 84 (2000) 39
40. E. Farnea et al., Nucl. Instr. Meth. A400 (1997) 87
41. Z. Hu et al., Phys. Rev. C60 (1999) 24315
42. M. Karny et al., Nucl. Instr. Meth. B126 (1997) 411
43. Ö. Skeppstedt et al., Nucl. Instr. Meth. A421 (1999) 521
44. P.M. Endt, Nucl. Phys. A633 (1998) 1
45. S. Lenzi et al., Proc. SM2K, Nucl. Phys. A, in print
46. J.A. Cameron et al., Phys. Rev. C49 (1994) 1347
47. E. Caurier et al., Phys. Rev. Lett. 75 (1995) 2466
48. H. Scheit et al., Phys. Rev. C60 (1999) 031301
49. J. Heese et al., Phys. Lett. B302 (1993) 390
50. G. Kraus et al., Phys. Rev. Lett. 73 (1994) 1173
51. A. Poves, Proc. 6th Int. Spring Seminar on Nuclear Physics - "Highlights of modern nuclear structure", ed. A. Covello, World Scientific, Singapore, 1999, p.129
52. G. Martinez-Pinedo et al., Phys. Rev. C53 (1996) R2602
53. D. Rudolph et al., Eur. Phys. J. A6 (1999) 377
54. G. Audi, A.H. Wapstra, Nucl. Phys. A624 (1997) 1
55. C. Baktash, contribution to this volume
56. E. Roeckl et al., Proc. ENPE 99, AIP Conf. Proc. 495 (1999) 63, R. Borcea et al., Proc. PINGST 2000, edts. D. Rudolph, M. Hellström, LUIP003, 2000, p.118 and to be published
57. A. Jokinen et al., private communication, to be published
58. D. Rudolph et al., Phys. Rev. Lett. 80 (1998) 3018
59. D. Rudolph et al., Phys. Scripta T88 (2000) 21
60. M. Górska et al., Phys. Rev. Lett. 79 (1997) 2415
61. M. Lipoglavšek et al., Phys. Lett. B440 (1998) 246

62. M. Palacz et al., Proc. SM2K, Nucl. Phys. A, in print
63. C. Fahlander et al., Phys. Rev. C63 (2001) 021307(R)
64. M. Chartier et al., Phys. Rev. Lett. 77 (1996) 2400
65. H. Grawe et al., Physica Scripta T56 (1995) 71
66. M. Górska et al., Proc. ENPE99, AIP Conf. Proc. 495 (1999) 217
67. H. Grawe et al., Proc. TOURS 2000, AIP Conf. Proc., in print
68. R. Grzywacz, Proc. ENAM98, AIP Conf. Proc., 481 (1999) 257
69. C. Baktash et al., Proc. SM2K, Nucl. Phys. A, in print
70. M. Górska et al., Phys. Rev. C58 (1998) 108
71. F.J. Gloeckner, F.J.D. Serduke, Nucl. Phys. A220 (1974) 477
72. R. Gross, A. Frenkel, Nucl. Phys. A267 (1976) 85
73. J. Blomqvist, L. Rydström, Physica Scripta 31 (1985) 31
74. X. Ji, B.H. Wildenthal, Phys. Rev. C37 (1988) 1256
75. J. Sinatkas et al., J. Phys. G18 (1992) 1377 and 1401
76. F. Andreozzi et al., Phys. Rev. C54 (1996) 1636
77. B.A. Brown, K. Rykaczewski, Phys. Rev. C50 (1994) 2270
78. L. Coraggio et al., J. Phys. G26 (2000) 1697
79. T. Werner et al., Z. Phys. A358 (1997) 169
80. Ch. Engelmann et al., Z. Phys. A352 (1995) 351
81. T. Motobayashi et al., Phys. Lett. B346 (1995) 9
82. E. Caurier et al., Phys. Rev. C58 (1998) 2033
83. N. Fukunishi et al., Phys. Lett. B296 (1992) 279
84. K.A. Mezilev et al., Phys. Scripta T56 (1995) 272
85. A. Huck et al., Phys. Rev. C31 (1985) 2226
86. S. Franchoo et al., Phys. Rev. Lett. 81 (1998) 3100
87. J.M. Daugas et al., Phys. Lett. B476 (2000) 213
88. H. Grawe et al., Proc. SM2K, Nucl. Phys. A, in print
89. R. Broda et al., Phys. Rev. Lett. 74 (1995) 868
90. J.I. Prisciandaro et al., Phys. Rev. C60 (1999) 031301 and 054307
91. W.F. Mueller et al., Phys. Rev. Lett. 83 (1999) 3613
92. W.F. Mueller et al., Phys. Rev. C61 (2000) 054308
93. O. Sorlin, Proc. NN2000, Strasbourg, to be published in Nucl. Phys. A
94. P.G. Reinhard et al., RIKEN Review 26 (2000) 23
95. V.I. Isakov et al., Physics of Atomic Nuclei 63 (2000) No. 10
96. K. Sistemich et al., Z. Phys. A285 (1978) 305
97. B. Fogelberg et al., Nucl. Phys. A429 (1984) 205
98. A. Korgul et al., Eur. Phys. J. A7 (2000) 167
99. C.T. Zhang et al., Z. Phys. A358 (1997) 9
100. M. Mineva et al., to be published
101. Pinston et al., Phys. Rev. C61 (2000) 024312
102. W. Urban et al., Eur. Phys. J. A5 (1999) 239
103. J.P. Omtvedt et al., Phys. Rev. Lett. 75 (1995) 3090